ICAS 2016
30th Congress of the International Council of the Aeronautical Sciences
DCC, Daejeon, Korea ; September 25-30, 2016

EXPERIMENTAL STUDY ON AERODYNAMIC LOAD CONTROL USING SYNTHETIC JET ACTUATORS

T.A. Berk[1, 2] and H.W.M. Hoeijmakers[1]
[1]Group Engineering Fluid Dynamics, University of Twente, Enschede, The Netherlands
[2]Faculty of Engineering and the Environment, University of Southampton, UK

Keywords: *Aerodynamics (Flow Control, Load Control, Wind Tunnel Testing)*

Abstract

This paper addresses the use of piezo-electric driven synthetic jet actuators as aerodynamic load control device in a 2D wing wind-tunnel model with a NACA0018 airfoil section with a chord of 0.165 m. Synthetic jets can be integrated in for instance wings and wind turbine blades to alleviate load variations and therewith reduce risk of fatigue damage. Compared to other flow control devices, synthetic jet actuators are favorable due to their small response time and low power requirements. A synthetic jet actuator from literature has been redesigned in order to fit inside the present airfoil section, at a location as closely as possible to the trailing edge of the airfoil. The jet exits from a narrow slot in the direction perpendicular to the surface of the airfoil. First, a prototype version of this redesigned actuator was manufactured and the jet velocity was measured using hot-wire anemometry. These measurements show that maximum centerline jet velocities up to 45 m/s can be achieved at an optimum actuation frequency of 700 Hz. Next, a non-swept 2D NACA0018 wing fitted with a module containing ten span wise distributed actuators was designed and manufactured. Wind tunnel tests have been performed in an open return wind tunnel at the University of Twente with a closed test section of 0.455 m by 0.455 m in cross section. The obtainable variation in the lift coefficient of the wing was measured, within some range of the actuation parameters. The highest relative increment in lift coefficient of 0.06 was obtained for a free-stream velocity of 12.4 m/s, combined with an actuation frequency of 750 Hz, corresponding to a reduced frequency of 10.

1 Introduction

Because aircraft and wing turbines operate in the uncontrolled outdoor environment, airplane wings and wind turbine blades are subjected to wind speed variations. As wings and blades grow in size, structural and fatigue loads caused by these variations become more pronounced [1]. Using a combination of sensors and actuators, the variation in incoming flow can theoretically be countered to keep blade and wing loading constant, reducing the risk of fatigue damage.

1.2 Flow Control

Controlling of the flow around an airfoil is known as flow control. An extensive overview of techniques and types of flow control is given by Gad-El-Hak [2]. Historically, emphasis has been put to control boundary layer transition. Delaying the transition from laminar to turbulent flow can potentially reduce skin-friction drag by an order of magnitude [2].

More recently, flow separation control has received much attention. An example of successful flow separation control, increasing the stall-angle of a NACA0018 wing by 22% and as a result the maximum lift coefficient by 11% is given by Koopmans [3]. Note that the actuators utilized in that work are similar to the actuators employed in the present study.

Another type of flow control is load control. By manipulating the streamlines around an airfoil at fixed (geometric) angle of attack, the circulation around the airfoil, and as a consequence the lift, is varied while maintaining the angle of attack of attack constant. This has the

same result as varying the effective (aerodynamic) angle of attack and is therefore also known as (virtual) pitch control. Active load control is the type of flow control addressed in the present research.

Different actuation techniques can be used for (active) load control. An overview is given by Johnson [1]. The most well-known techniques are pitching the configuration as a whole (generally used for wind turbine blades) and the traditional extension of slats and flaps (generally used for airplane wings). Other techniques include the micro-flap [4], micro-tab and micro-jet [5]. Most techniques control lift either by increasing the camber of the wing, or by creating a recirculation zone at the pressure side of the wing, near the trailing edge, increasing the effective camber of the wing.

1.2 Synthetic Jets

In the present research, synthetic jets are used as active load control devices. Synthetic jets (SJs) are created by actuators featuring alternating blowing and suction phases. These actuators consist of a cavity with an oscillating diaphragm on one side and an orifice or slot on one of the other sides. The orifice/slot forms the connection of the cavity with the wall over which the flow is to be manipulated. During the suction phase, fluid located at the wall is ingested through the orifice/slot into the cavity. During the blowing phase, this fluid is ejected, through the orifice/slot forming a vortex ring (or pair) at the edges of the slot. This vortical structure will be convected with the outside flow in combination with the self-induced velocity of the vortical structure. The cyclic blowing and suction creates a zero-net-mass-flux from the orifice/slot that has a zero mass flux but non-zero momentum flux. To obtain load control, SJs are located near the trailing edge of an airfoil, blowing perpendicular to the surface on the pressure side, creating a similar effect as micro-flaps, micro-tabs or micro-jets.

An important benefit of SJs is that they are formed entirely of the working fluid and therefore do not require a fluid supply with corresponding piping and pumps. The absence of moving mechanical parts (apart from the oscillating diaphragm inside the actuator) potentially makes the synthetic jet actuator much faster and more energy efficient than devices such as micro-tabs and micro-flaps.

The ejection of a train of vortices by a SJ into a crossflow can be characterized using three non-dimensional parameters [6]; the aspect ratio of the slot (AR), the reduced frequency (F^+) and the momentum coefficient (c_μ), defined as:

$$AR = l/d, \tag{1}$$

$$F^+ = f_{act}\, c / U_\infty \text{ and} \tag{2}$$

$$c_\mu = \rho_j u_j^2 d / \rho_\infty U_\infty^2 c, \tag{3}$$

respectively. Here l is the length of the slot in spanwise direction, d is the width of the slot in chordwise direction, f_{act} is the actuation frequency of the jet, c is the chord length of the wing, U_∞ is the freestream velocity, ρ_j and ρ_∞ are the density of the jet and the density of the freestream, respectively. Finally, u_j is the jet velocity averaged over the blowing phase of the cycle.

The time-averaged increase of the lift coefficient for different values of the reduced frequency, F^+, and momentum coefficient, c_μ, have been computed by de Vries [7]. These results are reproduced in Figure 1 and Figure 2.

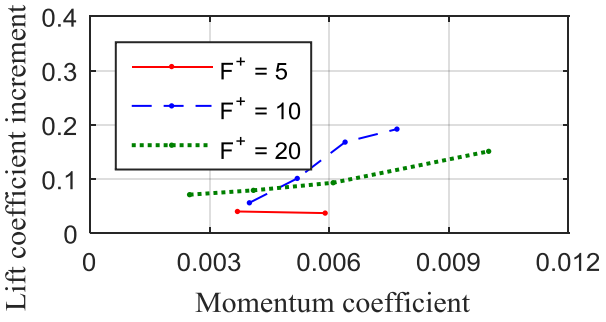

Fig. 1. Time-averaged increase in lift coefficient as function of momentum coefficient for a NACA0018 airfoil at Re_c = 550,000, M_∞ = 0.15, α = 0 deg, x_j/c = 0.88. Adapted from [7].

Figure 1 shows the increment in lift coefficient as function of the momentum coefficient c_μ for three values of the reduced frequency F^+. A reduced frequency of F^+ = 10 shows to have most potential to increase the lift coefficient. To be able to compare the experimental and computational results, a momentum coefficient of at least c_μ = 0.004 is preferred for the actuator designed in the present study.

Figure 2 shows the increment in the lift coefficient as function of the momentum coefficient c_μ for different chord wise locations (x_j/c) of the jet and angles of attack (α) of the wing. The difference between x_j/c = 0.88 (A) and x_j/c = 0.95 (B) clearly indicates that a jet position further towards the trailing edge leads to a higher increment in the lift coefficient. Therefore, the actuator is designed to be located as close to the trailing edge as possible.

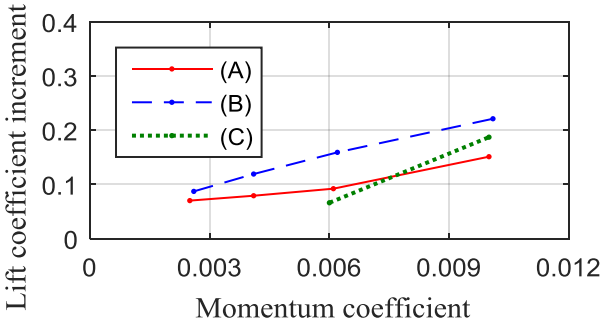

Fig. 2. Time-averaged increase in lift coefficient as function of momentum coefficient for a NACA0018 airfoil at Re_c = 550,000, M_∞ = 0.15, F^+ = 20. For x_j/c = 0.88, α = 0 deg (A), x_j/c = 0.95, α = 0 deg (B) and x_j/c = 0.95, α = 9 deg (C). Adapted from [7].

2 Prototype Actuator

The synthetic jet actuator employed in the present research is designed in such a way that it can be embedded in an airfoil for the purpose of aerodynamic load control. First a, stand-alone, prototype actuator has been designed, constructed and tested separately from the airfoil. The maximum jet velocity generated by this actuator has been measured for a range of the actuation parameters. This section discusses the design, manufacturing, testing and results of the prototype synthetic jet actuator.

2.1 Design

The synthetic jet actuator used in this study has been based on an actuator designed at the University of Florida by Oyarzun [8]. This actuator has also been used for the purpose of flow separation control in previous research at the University of Twente by Koopmans [3].

The design of the actuator is constrained by the size of the airfoil. Because the synthetic jet is situated close to the trailing edge the actuator thickness is limited. For this specified maximum thickness, a synthetic jet with a high momentum coefficient, c_μ, is desired. A high momentum coefficient, i.e. a high jet velocity, requires an actuator with a diaphragm resonance frequency close to the Helmholtz resonance frequency of the cavity/orifice geometry.

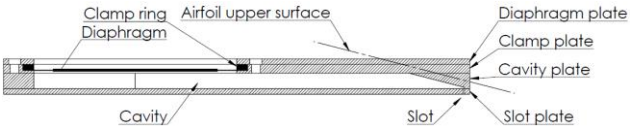

Fig. 3. Cross-sectional view prototype actuator.

A cross-sectional view of the actuator is shown in Figure 3. The actuator was kept as thin as possible, while keeping the Helmholtz resonance (calculated using the method described in [9]) and the diaphragm resonance coupled. An oblique inner wall of the cavity close to the slot (see Figure 3) enables placement of the actuator closer to the trailing edge of the airfoil.

The main dimensions of the designed actuator are:

-a slot width of d = 0.25 mm;
-a slot length of l = 30 mm;
-a slot height of h = 1 mm; and
-a cavity volume of V_c = 7300 mm^3.

The actuator is build up out of multiple plates as shown in Figure 4. This design was chosen for manufacturing reasons as well as in order to be able to clamp a piezoelectric diaphragm inside the actuator. The bimorph piezo diaphragm is a standard audio component (P412013T-JB) manufactured by APC International, Ltd. It is clamped with a custom manufactured stainless steel ring between four aluminum plates. All cavities were milled from the aluminum plates, except for the slot, which was machined using wire-cut electrical discharging.

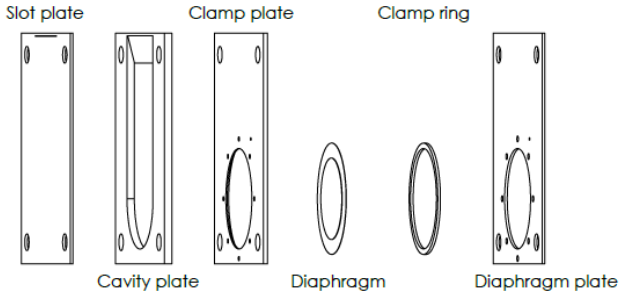

Fig. 4. Exploded view of prototype actuator

2.2 Experimental Setup

The jet velocity has been measured using a single-wire Dantec type 55P11 hot-wire, connected to a constant temperature Streamline 90N10 anemometer. The hot-wire has been calibrated using a Disa 55D44 pressure control unit attached to a nozzle. The pressure drop over the nozzle has been measured using a Betz 5000 micromanometer.

The hot-wire support was attached to a three-axes positioning table. Using this table the hot-wire could be traversed with an estimated precision of 0.05 mm, implying that a very precise grid of measuring points could be defined. However, the positioning of this grid relative to the slot was less precise. To get the wire as close to the slot as possible, while minimizing the disturbance of the airflow, the probe was placed at an angle of 45 deg relative to the actuator. To minimize the effect of the 1.25 mm length of the wire, it was positioned parallel to the slot.

2.3 Results

The velocity has been measured at the jet exit centerline first. Figure 5 shows an example of the velocity magnitude measured during a typical blowing cycle for f_{act} = 700 Hz, E_{act} = 100 V_{pp}.

The measured velocity shows noise peaks of typically one data point. To remove false maxima from this cycle, the velocity distribution is smoothened using a nine-point central averaging procedure. The smoothened velocity distribution is averaged over 1000 cycles to give a reliable representation of the variation of the velocity magnitude during a cycle. Since the actuator is a zero-net-mass-flux actuator, the velocity averaged over the slot area and actuator cycle are zero.

Because the data shown in Figure 5 has been taken a small distance (approximately 0.1 mm) above the slot, the velocity during the blowing part of the cycle is higher than the velocity measured during the suction part of the cycle. This corresponds to the phenomenon that a jet is formed during the blowing part of the cycle, which is directed out of the slot, while during the suction part of the cycle fluid is drawn into the slot from the sides [6]. In this study only the blowing part of the cycle (the first half as presented in Figure 5) is considered.

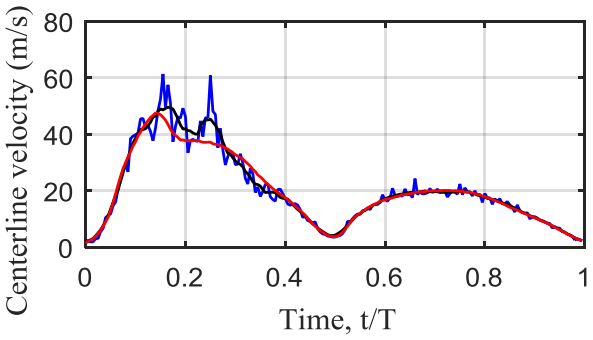

Fig. 5. Example of measured (——) and smoothened (——) velocity magnitude at jet exit centerline as function of time during one actuation cycle, as well as the smoothened velocity magnitude averaged over 1000 cycles (——) (f_{act} = 700 Hz, E_{act} = 100 V_{pp}).

The peak blowing velocity has been measured for a range of actuation frequencies f_{act} and voltages E_{act} the piezo-electric element is subjected to. Figure 6 presents the frequency response of the magnitude of the peak blowing velocity for the present prototype actuator, compared to that of two similar actuators from literature, for an actuation voltage of E_{act} = 100 V_{pp}.

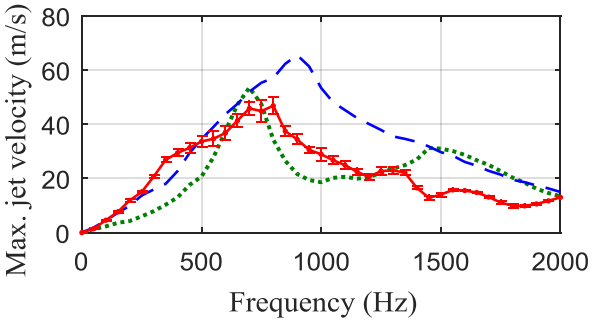

Fig. 6. Frequency response of prototype actuator (——), compared to that of actuator by Oyarzun [8] (·····) and that by Koopmans [3] (– –), all for E_{act} = 100 V_{pp}. The standard deviation for the prototype actuator is indicated by the error bars.

The actuator by Oyarzun [8] has been redesigned by Koopmans [3], such that the diaphragm and Helmholtz resonance frequencies are coupled as indicated by the merging of the peaks in the frequency response curve. In the present study, the actuator was redesigned to fit inside the airfoil as close as possible to the trailing edge of the airfoil. The comparison of the frequency response of [3] and that of the present

study in Figure 6 shows that for f_{act} > 500 Hz the coupling went at the expense of a drop in the maximum jet velocity. The maximum jet velocity dropped from 65.5 m/s at 900 Hz to 45.8 m/s at 700 Hz.

The effect of the actuation voltage E_{act} on the peak blowing velocity for f_{act} = 700 Hz is presented in Figure 7. The peak blowing velocity increases almost linearly with the actuation voltage up to approximately E_{act} = 100 V_{pp}, above which the effect of increasing the actuation voltage decreases. To obtain a high jet velocity while avoiding that the piezoelectric diaphragm is exposed to unnecessarily high stresses, an actuation voltage of E_{act} = 100 V_{pp} is considered ideal. This E_{act} is used in the remainder of the present study.

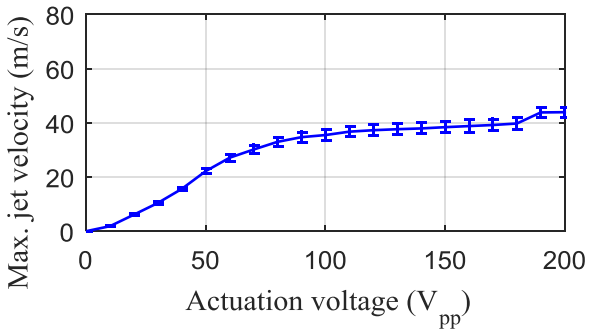

Fig. 7. Maximum centerline velocity as function of actuation voltage (f_{act} = 700 Hz). The error bars indicate the standard deviation.

The variation of the magnitude of the peak blowing velocity along the length (span) and along the width (chord) of the slot has also been measured. In spanwise direction the variation is very small over the central 85% of the slot. Near the edges, the boundary layer inside the slot and three-dimensional effects reduce the peak blowing velocity. In chordwise direction the small width (0.25 mm) implies that the boundary layer extends over the whole width, causing a channel-like velocity profile.

The development of the distribution of the magnitude of the velocity was measured on a grid with the spanwise position fixed at the center of the slot. The map of the development of the jet is presented in Figure 8. The jet centerline appears to be biased towards the negative y-direction at an angle of approximately 12 deg, which is towards the left in the orientation in Figure 3. It is assumed that this is caused by the oblique inner wall of the cavity as shown in Figure 3 and by the change in direction the flow makes just before exiting the actuator through the slot.

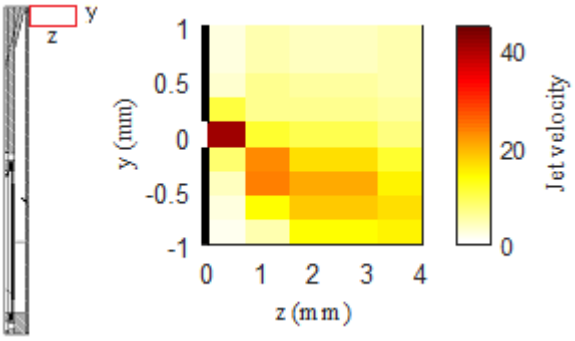

Fig. 8. Map of velocity magnitude in plane x = 0 for f_{act} = 700 Hz, E_{act} = 100 V_{pp}.

The momentum coefficient c_μ as given by Equation (3) is calculated based on the square of the jet velocity area-averaged over the area of the slot and time-averaged over a full blowing cycle. The momentum coefficient c_μ is presented in Figure 9 as function of the actuation frequency for three different values of the reduced frequency, all for E_{act} = 100 V_{pp}.

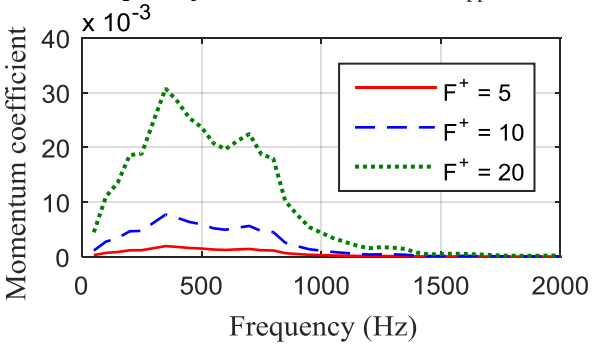

Fig. 9. Expected momentum coefficient versus actuation frequency for three values of the reduced frequency. E_{act} = 100 V_{pp}.

From Figure 1, based on data presented in [7], it was concluded that a reduced frequency of F^+ = 10 with a momentum coefficient of c_μ > 0.004 is preferred. Figure 9 indicates that the momentum coefficient for F^+ = 10 is above this threshold over a range of actuation frequencies. This implies that load control is feasible based on the described prototype actuator.

3 Integrated Actuator

The developed actuator has been fitted into a wind-tunnel model with a NACA0018 airfoil section. This straight (2D) wing has a chord c = 0.165 m and span b = 0.450 m. The centerline of the slot is located at the chordwise position of x_j/c = 0.975, i.e. very close to the trailing edge of the wing. In spanwise direction ten actuators are fitted, with their slots covering 67% of the span of the airfoil. The jet velocity has been re-measured to determine any differences with the performance of the prototype actuator. The changes in lift and drag caused by the action of the synthetic jets have been measured using a load balance. This section describes the design, manufacturing, testing as well as results obtained for the wing with integrated synthetic-jet actuators.

3.1 Design

In the design of the prototype actuator described above, it was already taken into account that the actuator had to be fitted inside the airfoil section. Therefore, the internal design of the integrated actuators is identical to the design of the prototype actuator.

Cross-sectional views as well as a picture of the side view of the airfoil section are presented in Figure 10. The forward part of an existing airfoil section was used, meaning that only the aft part had to be manufactured. For the actuator a plate-type of design, similar to the prototype actuator, was made. Now the oblique aft part of the cavity is part of the plate on the suction side of the airfoil. Furthermore, the slot plate and the cavity plate are combined in one plate, while the slots are located between two plates (the suction side plate and the pressure side plate) instead of a slot wire-cut out of one of the plates. All plates were milled out of aluminum, with the external sides having the same shape as the airfoil.

Figure 11 presents an exploded view of the rear half of the airfoil section, showing the position of ten actuators side-by-side in spanwise direction.

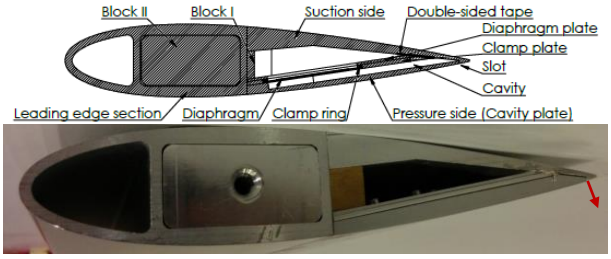

Fig. 10. Schematic of side-view and picture of actuators integrated in NACA0018 airfoil. The red arrow indicates the location and direction of the jet.

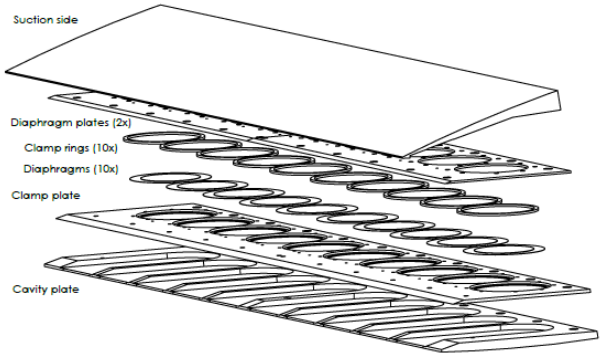

Fig. 11. Exploded view of of part of wind-tunnel model with ten integrated actuators

3.2 Experimental Setup

The jet velocity has been measured using the same hot-wire method as used for the prototype actuator described earlier. Lift, drag and pitching moment have been measured in the open blowdown wind tunnel facility at the University of Twente. A picture of this wind tunnel is presented in Figure 12, showing the contraction part and the 0.455 m by 0.455 m test section with the wind-tunnel model fitted vertically inside the test section. The three-component strain-gauge balance is situated underneath the test section. The wind tunnel has a velocity range of 7–25 m/s, with relatively high turbulence intensities of 1.5–2.0%. A boundary layer trip was applied on the leading edge of the wing to prevent the formation of a laminar separation bubble (even though laminar separation is not expected at these turbulence levels). The balance has been calibrated against known weights in the axial, normal and pitching moment directions. The freestream velocity was measured using a Pitot tube connected to a Digitron 2020P pressure transducer.

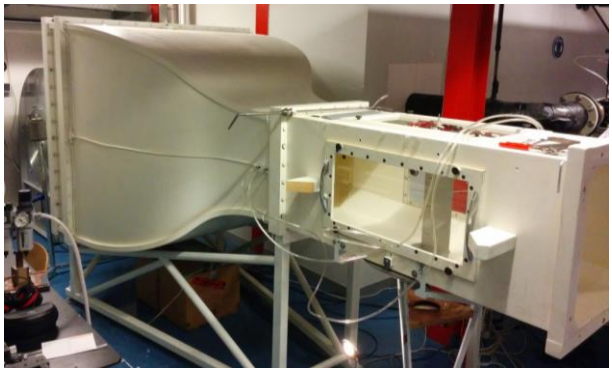

Fig. 12. Blow-down wind tunnel facility University of Twente.

3.3 Results

In this section, the results from the hot-wire measurements for the integrated actuators, still outside the wind tunnel, are presented and compared to results for the prototype actuator. Velocity measurements have been performed for all ten spanwise distributed actuators, which showed negligible differences between different actuators. This section also presents the load control results measured for the wind-tunnel model inside the wind tunnel.

3.3.1 Results Hot-Wire Anemometry

The frequency response of the maximum blowing velocity for E_{act} = 100 V_{pp} is presented in Figure 13. The response for the integrated actuators is compared to that of the prototype actuator. The result for the integrated actuator shows a double peak in the frequency response, indicating that the Helmholtz resonance frequency and diaphragm resonance frequency have been decoupled. It is assumed that this is caused by some unaccounted for deficiencies in the manufactured airfoil section. The decoupling of the resonance frequencies has led to a decreased maximum blowing velocity of 33.7 m/s at f_{act} = 450 Hz. Note that the jet velocity in the range f_{act} = 400–500 Hz has increased compared to that of the prototype actuator.

The spanwise and chordwise variations of the peak blowing velocity over the area of the slot, as well as the variation with actuation voltage, for the integrated actuator are similar to those for the prototype actuator.

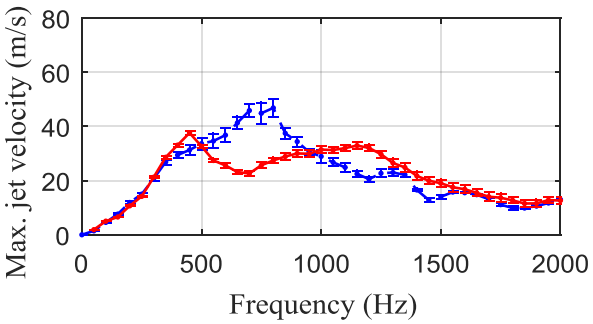

Fig. 13. Frequency response of integrated actuator (—•—) compared to that of prototype actuator (– –), both actuated at E_{act} = 100 V_{pp}. Standard deviations are indicated by errorbars.

The development of the jet at a fixed spanwise location, i.e. at the center of the slot, has been measured on a fine grid. This development is presented in Figure 14. Similar to the prototype actuator, the jet has a deviation towards the negative *y*-direction, which is towards the leading edge of the airfoil (i.e. in the direction opposite to the freestream).

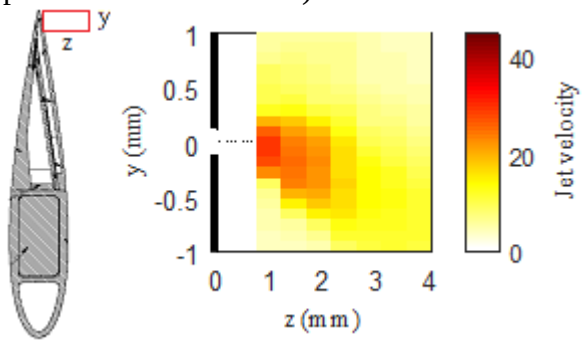

Fig. 14. Map of the velocity magnitude in the plane x = 0 for f_{act} = 1000 Hz, E_{act} = 100 V_{pp}.

To compare the development of the jet generated by the integrated actuators with that of the prototype jet, traverses of the peak blowing velocity at constant *z*-locations are plotted for both actuators in Figure 15. Although measured at different positions, this overlay shows the resemblance in the development of the jet produced by the prototype and that produced by the integrated actuators.

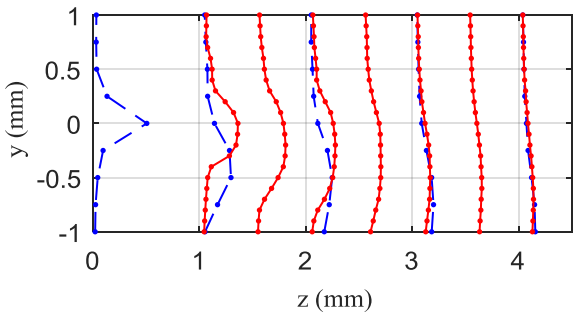

Fig. 15. Chordwise distribution of maximum jet velocity at a number of traverses z = constant in the plane x = 0. For the integrated actuator (——) f_{act} = 1000 Hz and E_{act} = 100 V_{pp}. For the prototype actuator (– –) f_{act} = 700 Hz and E_{act} = 100 V_{pp}.

The momentum coefficient, based on the square of the jet velocity averaged over the area of each slot and over a full blowing cycle as calculated by (3), is presented in Figure 16. Note that while the maximum peak blowing velocity for the integrated actuator is lower than that for the prototype actuator, the maximum momentum coefficient, for a given reduced frequency, is higher.

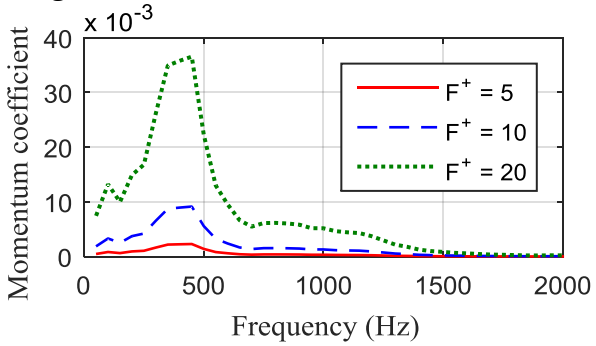

Fig. 16. Expected momentum coefficient as function of actuation frequency for F^+ = 5, F^+ = 10 and F^+ = 20. E_{act} = 100 V_{pp}.

3.3.1 Wind Tunnel Results

The loads on the airfoil section have been measured for actuated and for non-actuated cases for a number of values of the momentum coefficient and reduced frequency. For actuated cases the time-averaged increment (with respect to the corresponding value for the non-actuated case) in lift coefficient, Δc_l, is presented in Figure 17. As expected from the results by de Vries [7], shown in Figure 1, a reduced frequency of F^+ = 10 leads to the highest increment in lift coefficient. In general, Δc_l increases for increasing momentum coefficient, c_μ. For F^+ = 10, there is a maximum in Δc_l at c_μ = 0.0022. It is assumed that the lower Δc_l for higher momentum coefficients is caused by the low freestream velocities corresponding to these cases. These freestream velocities are close to the cut-in speed of the wind tunnel, leading to a high turbulence intensity and to velocity fluctuations.

The time-averaged increment in the drag coefficient is presented in Figure 18. The drag is slightly reduced for almost all cases. The cause of this decrease in drag coefficient is not clear.

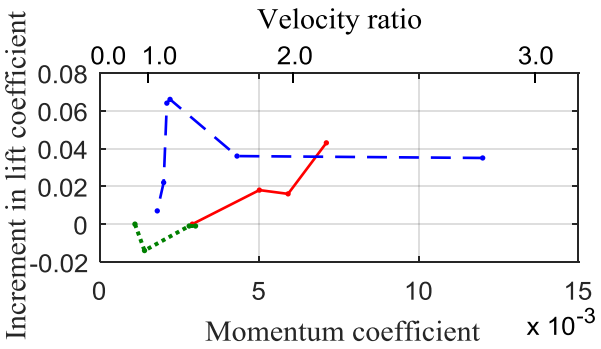

Fig. 17. Increment in lift coefficient as function of momentum coefficient for three values of reduced frequency; F^+ = 5 (——), F^+ = 10 (– –) and F^+ = 20 (·····), measured at α = 5 deg.

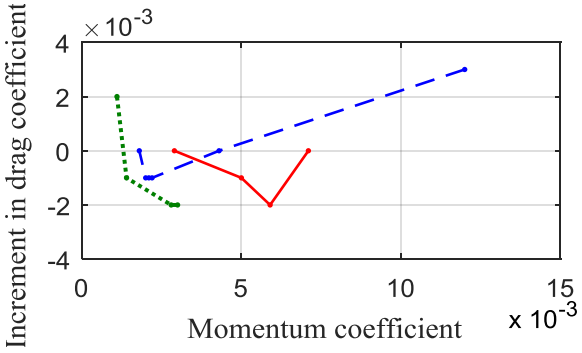

Fig. 18. Increment in drag coefficient as function of momentum coefficient for three values of reduced frequency; F^+ = 5 (——), F^+ = 10 (– –) and F^+ = 20 (·····), measured at α = 5 deg.

Figures 19 and 20 present the lift and drag coefficients as function of angle of for Re_c = 140,000, M_∞ = 0.04, F^+ = 10 and c_μ = 0.0021. Figure 19 compares the lift curve for unactuated and for the actuated flow. The actuation increases the lift coefficient slightly at every angle of attack. The drag coefficient, shown in Figure 20 is decreased at every angle of attack. Although the changes appear to be small, these re-

sults show that actuation using synthetic jets can be used for load control to increase (or decrease in case the actuator is on the upper side of the airfoil) the lift of an airfoil. An added benefit of drag reduction will render actuation more energy efficient.

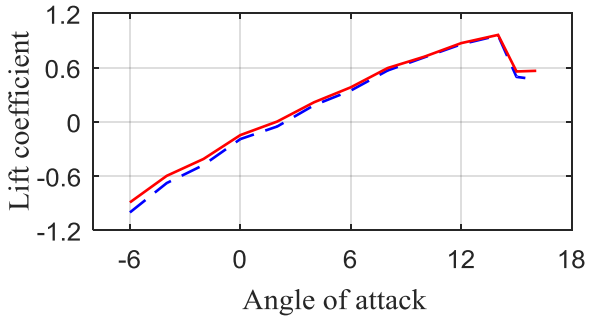

Fig. 19. Lift coefficient as function of angle of attack with (——) and without (– – –) actuation. Re_c = 140,000, M_∞ = 0.04, F^+ = 10 and c_μ = 0.0021.

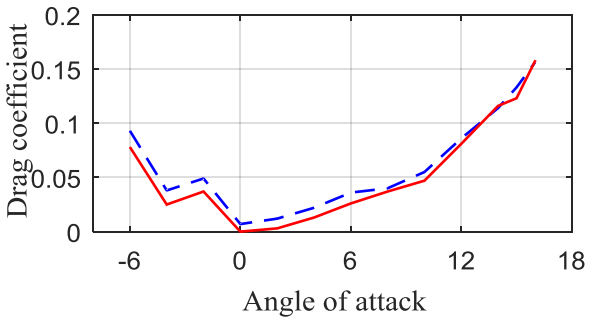

Fig. 20. Drag coefficient as function of angle of attack with (——) and without (– – –) actuation. Re_c = 140,000, M_∞ = 0.04, F^+ = 10 and c_μ = 0.0021.

4 Full-Scale Applications

The flow conditions used in the present study are different from flow conditions corresponding to real full-scale applications.

Scaling the results of the present research to the case of a full-scale application requires scaling of the geometrical parameters and scaling of the flow parameters. For the present research, scaling of the geometrical parameters implies that the chordwise slot location, x_j/c, the relative slot width, d/c, as well as the angle of attack, shape of the airfoil, the cavity and slot should be identical. Scaling of the flow parameters requires the Reynolds number, Re_c, Mach number M_∞, reduced frequency, F^+, and momentum coefficient, c_μ, to be identical.

Typical Reynolds numbers for a commercial airplane in cruise condition are of the order of $Re_c = 10^8$–10^9. The Reynolds number for the wind tunnel model in the present study is $Re_c = 0.14\times10^6$, which is a factor 10^4 lower than the full-scale Reynolds number. This difference in Reynolds number implies that the flow over the wind-tunnel model is mostly laminar, while the flow over a full-scale application is mostly turbulent. However, the flow in the wind tunnel as used in the present research has a high level of turbulence intensity, provoking early transition. This leads to the conclusion that this difference in Reynolds number is not expected to affect the results to a large extent.

The reduced frequency is $F^+ = f_{act}c/U_\infty$. The dimension of the airfoil section and the magnitude of the freestream velocity in the present research can be considered a factor 10–100 smaller than in full-scale applications. This implies that the actuation frequency for a full-scale application is of the same order as the actuation frequencies used in the present research.

The momentum coefficient c_μ scales with $u_j^2 d/(u_\infty^2\, c)$. If the relative slot width, d/c, is kept constant, an increase in freestream velocity of a factor of order ten also means a required increase in jet velocity of a factor of order ten. This is not considered to be realistic, given that the jet velocity in the present research has been u_j = 34 m/s. If the slot width would be increased to resolve this problem, it would be increasingly hard to generate a sufficiently high jet velocity.

In addition to the effect of scaling on the effect of the synthetic jets, the effect of scaling on the internal dynamics of the actuator is unknown. The Helmholtz and diaphragm resonance frequencies depend on the dimensions of the cavity, the slot and the diaphragm.

A geometrically scaled actuator would require a larger piezo-electric disc. It is unknown up to what diameters piezo discs can be manufactured. The maximum diameter found in literature is 55 mm (GREWUS GmbH), which is not much larger than the 41 mm diameter used in the present study.

5 Conclusions

The present study has addressed the use of piezo-electric driven synthetic jet actuators as aerodynamic load control device inside a 2D NACA0018 airfoil with a chord of c.= 0.165 m. Results of numerical simulations from literature indicated an increase in load control potential for a chordwise slot location as close as possible to the trailing edge. A synthetic jet actuator from literature, used in an earlier study, has been redesigned to decrease its height, such that it fits inside the airfoil with its slot centerline at x_j/c = 0.975.

A prototype of this redesigned synthetic jet actuator has been manufactured in order to measure the maximum jet velocity achieved by the actuator. The maximum jet velocity of the prototype actuator is u_j = 46 m/s at an optimum actuation frequency of f_{act} = 700 Hz and an actuation voltage of E_{act} = 100 V_{pp}. The actuator used in previous research that formed the basis for the design of the present actuator had a maximum jet velocity of u_j = 65 m/s at f_{act} = 900 Hz. The frequency response of the present actuator is less favorable than that of the previous actuator due to differences in the interior of the actuator. As a consequence, the maximum jet velocity has decreased by 30%.

A 2D non-swept wing with NACA0018 airfoil section, with a chord of c = 0.165 m and a span of b = 0.45 m, spanning the wind-tunnel height, has been designed. The airfoil contains ten spanwise distributed synthetic jet actuators. The slots extend over 67% of the span of the full wing span. The geometry of the cavity and the slot of the embedded actuators is similar to the geometry of the cavity and slot of the prototype actuator. Due to deficiencies caused by the manufacturing process, there are some differences between the prototype actuator and the embedded actuators. These differences have unfortunately resulted in a decoupling of the Helmholtz resonance frequency and diaphragm resonance frequency. As a result, the maximum jet velocity has decreased to u_j = 34 m/s at an optimum actuation frequency of f_{act} = 450 Hz. However, the maximum momentum coefficient of the embedded actuator has increased compared to that of the prototype actuator.

Wind-tunnel measurements have shown an increment in the lift coefficient, Δc_l, when the synthetic jet actuators are activated. The maximum increment in the lift coefficient is Δc_l = 0.06 for a reduced frequency of F^+ = 10 and a momentum coefficient of c_μ = 0.0021. In addition to this increment in lift coefficient, the drag coefficient is decreased by the actuation, leading to a favorable efficiency of the actuation. The freestream velocity for this measurement was U_∞ = 12.4 m/s, corresponding to Re_c = 140,000 and M_∞= 0.04. From these results, it can be concluded that load control using synthetic jet actuators embedded in an airfoil section is viable.

References

[1] Johnson SJ, Baker JP, van Dam CP and Berg D. An overview of active load control techniques for wind turbines with an emphasis on microtabs. *Wind Energy*, Vol. 13, pp 239-253, 2010.

[2] Gad-El-Hak M. *Flow control, passive, active, and reactive flow management.* Cambridge University Press, 2000.

[3] Koopmans E and Hoeijmakers HWM. Experimental research on flow separation control using synthetic jet actuators. *Proceedings. 29th Congress of International Council of Aeronautical Sciences (ICAS2014)*. St. Petersburg, Russia, September 7-12 2014. Paper ICAS2014-0694, 2014.

[4] Chow R and van Dam C. On the temporal response of active load control devices. *Wind Energy*, Vol. 13, pp. 135-149, 2010.

[5] Blaylock M, Chow R and van Dam CP. Comparison of microjets with microtabs for active aerodynamic load control. *5th Flow control conference*, Chicago, Il, 2010. AIAA Paper 2010-4409, 2010.

[6] Glezer A and Amitay M. Synthetic jets. *Annual Review Fluid Mechanics*, Vol. 34, pp. 503-529, 2002.

[7] De Vries H. *On synthetic jet actuation for aerodynamic load control*. PhD thesis, University of Twente, 2013.

[8] Oyarzun MA and Cattafesta L. Design and optimization of piezoceramic zero-net mass-flux actuators. *Proc. 5th AIAA Flow Control Conference*, Chicago, Illinois, USA, AIAA Paper 2010-4414, 2010

[9] Chanaud RC. Effects of geometry on the resonance frequency of Helmholtz resonators. *Journal of Sound and Vibration*. Vol. 178(3), pp. 337-348, 1994.

Contact Author Email Address

mailto:h.w.m.hoeijmakers@utwente.nl

Copyright Statement